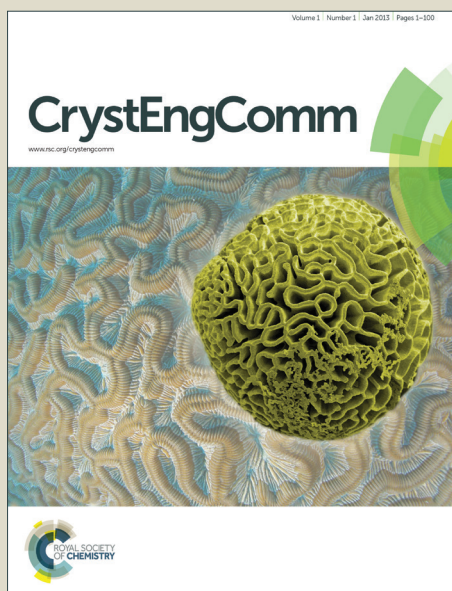


# CrystEngComm

Accepted Manuscript



This is an *Accepted Manuscript*, which has been through the Royal Society of Chemistry peer review process and has been accepted for publication.

*Accepted Manuscripts* are published online shortly after acceptance, before technical editing, formatting and proof reading. Using this free service, authors can make their results available to the community, in citable form, before we publish the edited article. We will replace this *Accepted Manuscript* with the edited and formatted *Advance Article* as soon as it is available.

You can find more information about *Accepted Manuscripts* in the [Information for Authors](#).

Please note that technical editing may introduce minor changes to the text and/or graphics, which may alter content. The journal's standard [Terms & Conditions](#) and the [Ethical guidelines](#) still apply. In no event shall the Royal Society of Chemistry be held responsible for any errors or omissions in this *Accepted Manuscript* or any consequences arising from the use of any information it contains.

## COMMUNICATION

## Facile synthesis of high-quality Pt nanostructures with controlled aspect-ratio for methanol electro-oxidation

Cite this: DOI: 10.1039/x0xx00000x

Yi Li, Ting Bian, Jingshan Du, Yalin Xiong, Fangwei Zhan, Hui Zhang,\* and Deren Yang

Received 00th January 2012,  
Accepted 00th January 2012

DOI: 10.1039/x0xx00000x

www.rsc.org/

**High-quality Pt nanobars with controlled aspect-ratio were synthesized by varying the amount of formaldehyde in benzyl alcohol containing oleylamine and exhibited substantially enhanced electrocatalytic properties for methanol oxidation relative to the commercial Pt/C.**

Platinum (Pt) is a key component of many catalysts used for a large number of reactions in many industrial processes and commercial devices due to its remarkable activity.<sup>[1]</sup> It is clear that the catalytic property of a Pt nanocrystal is strongly affected by its shape, which determines the arrangements of atoms on the surface.<sup>[2]</sup> The last decade has witnessed the successful synthesis of Pt nanocrystals in a rich variety of shapes, with notable examples including cubes, octahedrons, tetrahedrons, decahedrons, icosahedrons, rods, multipods, tetrahexahedrons, and concave cubes.<sup>[3]</sup> Among these shapes, well-controlled nanocubes made of Pt and exposed by {100} facets are particularly interesting due to their unique properties in different catalytic reactions. For example, Pt nanocubes enclosed with {100} facets were observed to enhance ring-opening ability for pyrrole hydrogenation and thus showed a higher selectivity to *n*-butylamine as compared to nanopolyhedra exposed by a mix of {111} and {100} facets.<sup>[4]</sup> In addition, the electro-oxidation of methanol was also found to be more active on Pt {100} facets relative to {111} facets.<sup>[5]</sup> As such, there is a strong effort to synthesize Pt nanocubes in a controlled manner to tailor their catalytic properties.<sup>[6]</sup> In general, the use of capping agent provides a facile and effective approach to the synthesis of Pt nanocubes by selectively stabilizing the {100} facets through preferential chemisorptions. To this end, Yang and co-workers demonstrated the synthesis of Pt nanocubes with cetyltrimethylammonium bromide (CTAB) as a capping agent by reducing  $K_2PtCl_4$  with  $NaBH_4$  in an aqueous solution.<sup>[7]</sup> Recently, high-quality Pt nanocubes have been successfully generated through an oil-phase approach in the presence of a trace amount of metal carbonyls<sup>[8]</sup> or with pure CO as a capping agent.<sup>[9]</sup> However, most of these reports inevitably involve the contamination of second metal in the final product or the use of very toxic gas.

Similar to a nanocube, a nanobar is characterized by six main side faces bounded by all {100} facets except for its anisotropic structure with aspect-ratio (length to width) larger than one. As

constrained by their highly symmetric face-centered cubic (*fcc*) lattice, only a few nanobars made of noble metals including Ag, Pd, and a combination of them were successfully generated through localized oxidative etching,<sup>[10]</sup> particle coalescence,<sup>[11]</sup> or kinetic control<sup>[12]</sup> to break the symmetry limitation. For a system involving Pt, it still remains a grand challenge to synthesize the nanobars, especially for tuning their aspect-ratio. Here, we report a facile approach to the synthesis of Pt nanobars with controlled aspect-ratio in benzyl alcohol containing oleylamine (OAm) and formaldehyde. The carbon supported Pt nanobars were evaluated as electrocatalysts for methanol oxidation and showed substantially enhanced performance in terms of activity and resistance to CO poison relative to the commercial Pt/C.

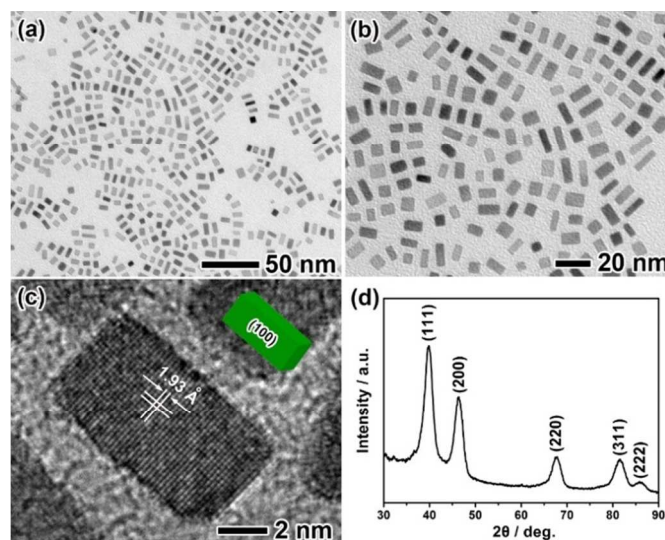


**Fig. 1** (a, b) TEM images, (c) HRTEM image, and (d) XRD pattern of the Pt nanobars prepared using the standard procedure. The inset in (c) shows the 3D model of a nanobar.

The synthetic procedure involved the reduction of  $Pt(acac)_2$  with benzyl alcohol at 180 °C in the presence of OAm and different amount of formaldehyde serving as capping agents (see Supporting Information for the details). Figure 1, a and b shows transmission

electron microscopy (TEM) images of the Pt nanobars prepared using the standard procedure (i.e., 0.1 mL of OAm and 1.5 mL of formaldehyde). These TEM images clearly show that most of the nanocrystals had a rectangle profile due to the projection along the  $\langle 100 \rangle$  zone axis. Unlike the five-fold twinned nanorods, these nanocrystals exhibited a homogeneous contrast from TEM observation, implying the formation of a bar-shaped structure. The average aspect-ratio, length, and width of the nanobars were measured to be 1.54, 7.03 nm, and 4.9 nm, respectively (Figure S1). The data were obtained from about 500 nanocrystals randomly selected from TEM images. The typical high-resolution TEM (HRTEM) image (Figure 1c) of an individual nanobar shows well-resolved, ordered fringes in the same orientation, indicating a single crystal. The fringes with a lattice spacing of 1.93 Å can be indexed to the  $\{200\}$  planes of Pt with a *fcc* structure. On the basis of TEM and HRTEM analyses, we can propose a three-dimensional (3D) model for the Pt nanobars as shown in the inset of Figure 1c. Figure 1d shows X-ray diffraction (XRD) pattern of the Pt nanobars. All the diffraction peaks can be indexed to the *fcc* Pt (JCPDS No. 04-0802). The broadening of the diffraction peaks can be attributed to the small size of the Pt nanobars.

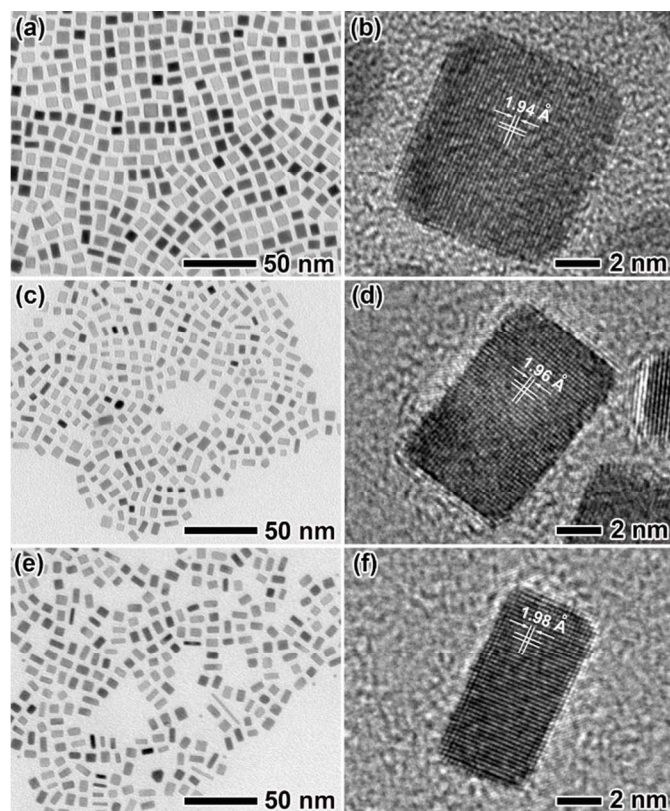


**Fig. 2** TEM and HRTEM images of the Pt nanobars prepared using the standard procedure, except for different amount of formaldehyde: (a, b) 0.5, (c, d) 1, and (e, f) 2 mL.

The aspect-ratio of Pt nanobars was readily tuned by varying the amount of formaldehyde. From the TEM images in Figure 2, a, c, and e, the aspect-ratio of the Pt nanobars gradually increased with the amount of formaldehyde fed in the synthesis. This demonstration was also supported by the corresponding HRTEM images (Figure 2 b, d, and f). The statistical data in Figure S2 show that both the average length and width of Pt nanobars decreased with increase of the amount of formaldehyde. However, the average width decreased much more rapid than the average length, leading to the

enhancement of the aspect-ratio. The strong capping capability of formaldehyde on the surface of Pt nanobars was responsible for the decrease of their length and width through inhibiting the growth.<sup>[13]</sup> When the amount of formaldehyde increased to 2 mL, the average aspect-ratio, length, and width of the Pt nanobars almost remained unchanged. Therefore, the amount of formaldehyde played a key role in controlling the aspect-ratio of Pt nanobars.

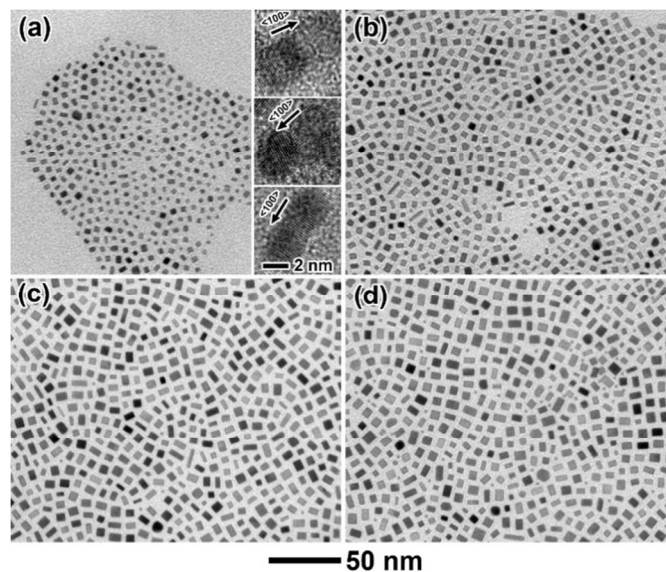


**Fig. 3** TEM images of the Pt nanocrystals prepared using the standard procedure, except for different period of reaction: (a) 0.5, (b) 1, (c) 3, and (d) 9 h. The insets in (a) correspond to the HRTEM images.

In order to understand the formation mechanism of Pt nanobars, a series of samples obtained using the standard procedure except for different reaction times were collected for TEM observation. From Figure 3a ( $t = 0.5$  h), numerous cubes of  $\sim 3$  nm in size together with a large number of small nanoparticles were initially formed. Careful observation from the HRTEM images (inset of Figure 3a) clearly shows the coalescence between two adjacent nanoparticles by sharing a common crystallographic orientation along the  $\langle 100 \rangle$  direction. As the reaction continued (Figure 3, b-d), most of nanocubes were gradually elongated along one of the axes (i.e., the  $\langle 100 \rangle$  direction) to form nanobars with aspect-ratios larger than one. As such, the particle coalescence was responsible for the formation of the Pt nanobars due to the obligation to minimize the surface energy of a system under thermodynamic control. A similar mechanism was also suggested for the formation of Pd nanobars in an aqueous solution.<sup>[11]</sup> However, the higher chemical stability of Pt relative to Pd require the larger driving force for the coalescence growth, and thus the different reaction system.<sup>[3c]</sup> In addition to the particle coalescence mechanism, the use of OAm and formaldehyde was also indispensable for the formation of the high-quality Pt nanobars. In the absence of both OAm and formaldehyde, the final product was dominated by the Pt icosahedrons enclosed with  $\{111\}$  facets (Figure S3a). Interestingly, the addition of formaldehyde could facilitate the formation of the nanobars (see Figure S3b), indicating that formaldehyde acted as a surface capping agent to stabilize the  $\{100\}$  facets of the Pt nanocrystals. However, careful observation shows the coexistence of a small amount of cuboctahedrons and five-fold twinned nanorods in the presence of only formaldehyde. When formaldehyde was substituted with acetaldehyde, the reactions also led to the formation of Pt nanobars (Figure S4), further indicating the correlation of the bar-shaped structure formation to the aldehyde group. When only OAm was

added, Pt tended to form nanocubes and five-fold twinned nanorods, both of them were mainly bound by {100} facets. This result reveals that OAm also favored the formation of Pt{100} facets serving as a capping agent, which was in agreement with the previous report.<sup>[6b]</sup> This demonstration was also supported by the TEM observation when replacing OAm with other amines (see Figure S5). Taken together, the selective co-adsorption of aldehyde and amine group on Pt{100} facets eventually facilitates the formation of high-quality Pt nanobars. In addition, the variation on the aspect-ratio of the Pt nanobars could be attributed to its capping capability associated with the amount of formaldehyde.

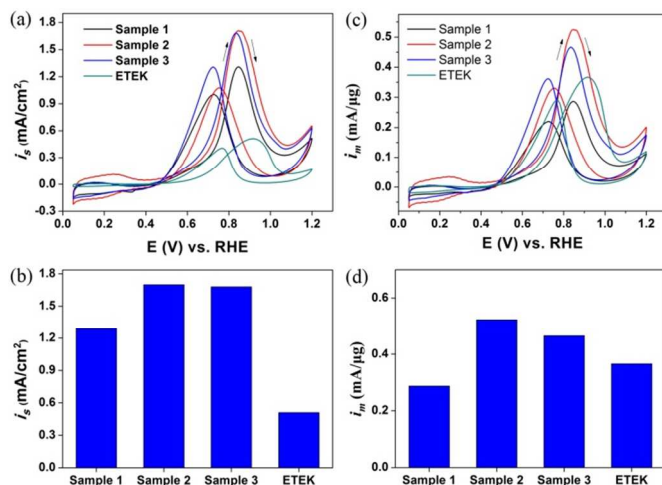


**Fig. 4** (a, b) Specific activities and (c, d) mass activities of methanol oxidation on three Pt nanobars with different aspect-ratios in 0.1 M HClO<sub>4</sub>/0.5 M methanol solution at a sweeping rate of 50 mV/s, including commercial Pt/C.

The Pt nanobars with three different aspect-ratios (i.e., 1.29, 1.45, and 1.54) were loaded onto a carbon black support (Vulcan XC-72) and then evaluated as electrocatalysts for methanol oxidation (MOR). To simplify the description, these three catalysts were denoted as Sample 1, Sample 2, and Sample 3, respectively. We benchmarked their electrocatalytic activity against the commercial Pt/C catalyst (E-TEK). Figure S6 shows cyclic voltammograms (CVs) of these four catalysts recorded at room temperature in an Ar-purged 0.1 M HClO<sub>4</sub> aqueous solution at a sweep rate of 50 mV/s. The electrochemically active surface area (ECSA) was calculated by measuring the charges collected in the H adsorption region from 0.05 to 0.4 V. The three Pt nanobars exhibited similar ECSAs with values of 21.9, 30.7, and 27.7 m<sup>2</sup>/g, respectively (see Table S1), which were much smaller than that of commercial Pt/C (71.7 m<sup>2</sup>/g), probably due to the remained organic species (e.g., OAm and benzyl alcohol) adsorbed on the surfaces of such nanocrystals and the size effects. Figure 4a shows CVs of these four catalysts for MOR at room temperature in an aqueous solution containing 0.1 M HClO<sub>4</sub> and 0.5 M methanol at a sweep rate of 50 mV/s. In general, the  $I_f/I_b$  ratio value (in which  $I_f$  and  $I_b$  are the forward and backward current densities, respectively) is used to evaluate the poisoning tolerance of the catalyst to the carbonaceous species.<sup>[14]</sup> Compared to the commercial Pt/C (1.24), all three Pt nanobars catalysts showed the higher  $I_f/I_b$  ratio value with a sequence of Sample 2 (1.6) > Sample 1 (1.32) > Sample 3 (1.29). The CO stripping was used to study the adsorption of CO on Pt surface, as the bonding strength of CO on Pt sites can be directly correlated to the change of potential position due to the oxidation (Fig. S7). For commercial Pt/C, this oxidation peak locates at 0.84 V, while all the Pt nanobars have the oxidation

peak below 0.8 V. These observations further confirm that the Pt nanobars have higher CO poisoning tolerance than the commercial Pt/C. In addition, these three {100}-cased nanobars also exhibited a remarkably higher specific activity towards MOR relative to the Pt/C (E-TEK) covered by mixed {111} and {100} facets. This result indicated that the {100} facets offered a higher MOR activity than the {111} facets, which was consistent with the previous report.<sup>[5]</sup> After being normalized over the ECSAs, their peak current densities in the forward anodic scan were singled out, as shown in Figure 4b. It is clear that the Pt nanobars with aspect-ratios of 1.45 (Sample 2) and 1.54 (Sample 3) show the highest forward current density (1.70 vs 1.68 mA/cm<sup>2</sup>) for MOR, which is 1.3 and 3.3 times higher than those of Sample 1 and commercial Pt/C, respectively. In addition, the mass activities of Samples 2 and 3 are also higher than that of the commercial Pt/C. The different electrocatalytic performance of the Pt nanobars with different aspect-ratios can be attributed to the size effect. The size of the Pt nanobars in Samples 2 and 3 was much smaller than that in Sample 1, resulting in the higher electrocatalytic activity toward MOR.

## Conclusions

We have demonstrated a facile approach for the synthesis of the Pt nanobars in high-quality with both OAm and formaldehyde as capping agents. The aspect-ratio of the Pt nanobars was simply tuned by varying the amount of formaldehyde fed in the synthesis. When supported on carbon, the Pt nanobars exhibited enhanced electrocatalytic activity and CO poisoning tolerance for MOR relative to the commercial Pt/C probably due to the facet and size effects. The high-quality Pt nanobars can be further used as seeds to construct various bimetallic nanocrystals with a complex structure, thereby opening up new opportunities to design advanced catalysts with enhanced performance for a rich variety of potential applications.

## Notes and references

State Key Lab of Silicon Materials, Department of Materials Science and Engineering, and Cyrus Tang Center for Sensor Materials and Applications, Zhejiang University, Hangzhou, Zhejiang 310027, P. R. China. E-mail: msezhanghui@zjue.edu.cn; TEL: 86-571-87953190; FAX: +86-571-87952322.

Electronic Supplementary Information (ESI) available: [details of any supplementary information available should be included here]. See DOI: 10.1039/c000000x/

- 1 a) W. Yu, M. Porosoff and J. Chen, *Chem. Rev.*, 2012, **112**, 5780-5817; b) M. Bowker, *Chem. Soc. Rev.*, 2008, **37**, 2204-2211; c) M. Debe, *Nature*, 2012, **486**, 43-51.
- 2 a) Y. Xia, Y. Xiong, B. Lim and S. Skrabalak, *Angew. Chem. Int. Ed.*, 2009, **48**, 60-103; b) Z. Quan, Y. Wang and J. Fang, *Acc. Chem. Res.*, 2013, **46**, 191-202; c) D. Wang and Y. Li, *Adv. Mater.*, 2011, **23**, 1044-1060.
- 3 a) T. Ahmadi, Z. Wang, T. Green, A. Henglein and M. El-Sayed, *Science*, 1996, **272**, 1924-1926; b) Y. Kang, J. Pyo, X. Ye, R. Diaz, T. Gordon, E. Stach and C. Murray, *ACS Nano*, 2013, **7**, 645-653; c) Z. Peng and H. Yang, *Nano Today*, 2009, **4**, 143-164; d) J. Chen, T. Herricks, M. Geissler and Y. Xia, *J. Am. Chem. Soc.*, 2004, **126**, 10854-10855; e) N.

- Tian, Z. Zhou, S. Sun, Y. Ding and Z. Wang, *Science*, 2007, **316**, 732-735; f) X. Huang, Z. Zhao, J. Fan, Y. Tan and N. Zheng, *J. Am. Chem. Soc.*, 2011, **133**, 4718-4721.
- 4 C. Tsung, J. Kuhn, W. Huang, C. Aliaga, L. Hung, G. Somorjai and P. Yang, *J. Am. Chem. Soc.*, 2009, **131**, 5816-5822.
- 5 E. Herrero, K. Franaszczuk and A. Wieckowski, *J. Phys. Chem.*, 1994, **98**, 5074-5083.
- 6 a) K. Bratlie, H. Lee, K. Komvopoulos, P. Yang and G. Somorjai, *Nano Lett.* 2007, **7**, 3097-3101; b) G. Chen, Y. Tan, B. Wu, G. Fu and N. Zheng, *Chem. Commun.*, 2012, **48**, 2758-2760; c) Z. Peng, C. Kisielowski and A. Bell, *Chem. Commun.*, 2012, **48**, 1854-1856; d) J. Ren and R. Tilley, *J. Am. Chem. Soc.*, 2007, **129**, 3287-3291; e) Y. Lee, S. Han, D. Kim and K. Park, *Chem. Commun.*, 2011, **47**, 6296-6298.
- 7 H. Lee, S. Habas, S. Kweskin, D. Butcher, G. Somorjai and P. Yang, *Angew. Chem. Int. Ed.*, 2006, **45**, 7824-7828.
- 8 a) C. Wang, H. Daimon, Y. Lee, J. Kim and S. Sun, *J. Am. Chem. Soc.*, 2007, **129**, 6974-6975; b) J. Zhang and J. Fang, *J. Am. Chem. Soc.*, 2009, **131**, 18543-18547; c) S. Lim, I. Ojea-Jimenez, M. Varon, E. Casals, J. Arbiol and V. Puntes, *Nano Lett.*, 2010, **10**, 964-973; d) R. Loukrakpam, P. Chang, J. Luo, B. Fang, D. Mott, I. Bae, H. Naslund, M. Engelhard and C. Zhong, *Chem. Commun.*, 2010, **46**, 7184-7186.
- 9 a) Y. Kang, X. Ye and C. Murray, *Angew. Chem. Int. Ed.* 2010, **49**, 6156-6159; b) B. Wu, N. Zheng and G. Fu, *Chem. Commun.*, 2011, **47**, 1039-1041.
- 10 a) Y. Xiong, H. Cai, B. Wiley, J. Wang, M. Kim and Y. Xia, *J. Am. Chem. Soc.*, 2007, **129**, 3665-3675; b) B. Wiley, Y. Chen, J. McLellan, Y. Xiong, Z. Li, D. Ginger and Y. Xia, *Nano Lett.* 2007, **7**, 1032-1036.
- 11 B. Lim, H. Kobayashi, P. Camargo, L. Allard, J. Liu and Y. Xia, *Nano Res.* 2010, **3**, 180-188.
- 12 J. Zeng, C. Zhu, J. Tao, M. Jin, H. Zhang, Z. Li, Y. Zhu and Y. Xia, *Angew. Chem. Int. Ed.* 2012, **51**, 2354-2358.
- 13 L. Zhang, D. Chen, Z. Jiang, J. Zhang, S. Xie, Q. Kuang, Z. Xie and L. Zheng, *Nano Res.* 2012, **5**, 181-189.
- 14 Z. Liu, X. Ling, X. Su, J. Lee, *J. Phys. Chem. B* 2004, **108**, 8234-8240.